IOPscience Journals Books Login Search Article lookup

Journal of Physics D: Applied Physics > Volume 46 > Number 23
Hyeon Jun Ha *et al* 2013 *J. Phys. D: Appl. Phys.* **46** 235102 doi:10.1088/0022-3727/46/23/235102

Flexible low-voltage pentacene memory thin-film transistors with combustion-processable Al_2O_3 gate dielectric and Au nanoparticles

Hyeon Jun Ha, Shin Woo Jeong, Tae-Yeon Oh, Minseok Kim, Kookhyun Choi, Jung Ho Park and Byeong-Kwon Ju
Show affiliations

Tag this article PDF (2.01 MB) View article

Abstract | References | Metrics

Paper

A Au nanoparticles (NPs) embedded pentacene thin-film transistor (TFT) with solution-based Al_2O_3 was fabricated on a polyethersulfone substrate. The TFT for low-voltage operation within −3 V was realized with the Al_2O_3 dielectric film. By a combustion process for Al_2O_3, efficient driving of conversion reaction at low annealing temperature of 200 °C can be achieved and the device can be made on a plastic substrate. And, the Au NPs were deposited by the contact printing method using the polydimethylsiloxane stamp. From the electrical characteristics of the devices, a saturation mobility value of 4.25 $cm^2 V^{-1} s^{-1}$, threshold voltage (V_{th}) of ~0.5 V, subthreshold swing of 70 mV dec^{-1} and memory window of 0.21 V at −3 V programming gate bias voltage were obtained.

Quadrupole Mass Spectrometers for Vacuum, Gas, Plasma and Surface Science
HIDEN ANALYTICAL www.HidenAnalytical.com

PACS
85.30.Tv Field effect devices
81.40.Ef Cold working, work hardening; annealing, post-deformation annealing, quenching, tempering recovery, and crystallization
85.35.-p Nanoelectronic devices
85.30.De Semiconductor-device characterization, design, and modeling
77.55.+f Dielectric thin films
82.33.Vx Reactions in flames, combustion, and explosions

Subjects
Electronics and devices

Related Articles

1. Improved Performance of Organic Thin Film Transistor with an Inorganic Oxide/Polymer Double-Layer Insulator
2. Extensive Leakage Current Reduction in Polymer Dielectric Thin Film by Metal Nanoparticles Incorporation for Organic Thin Film Transistor
3. A flexible organic active matrix circuit fabricated using novel organic thin film transistors and organic light-emitting diodes

More

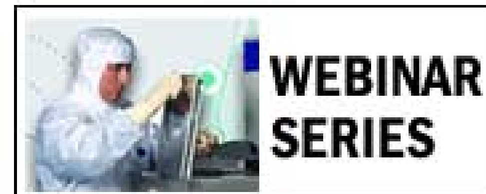

Related Review Articles

1. Graphene field-effect transistors
2. Field-effect transistors based on two-dimensional materials for logic applications

Share

Post to CiteUlike
Post to Bibsonomy

iopscience.iop.org

Home Search Collections Journals About Contact us My IOPscience

Flexible low-voltage pentacene memory thin-film transistors with combustion-processable Al_2O_3 gate dielectric and Au nanoparticles

This content has been downloaded from IOPscience. Please scroll down to see the full text.

2013 J. Phys. D: Appl. Phys. 46 235102

(http://iopscience.iop.org/0022-3727/46/23/235102)

View the table of contents for this issue, or go to the journal homepage for more

Download details:

IP Address: 163.152.52.92
This content was downloaded on 19/03/2014 at 00:50

Please note that terms and conditions apply.

J. Phys. D: Appl. Phys. **46** (2013) 235102 (7pp) doi:10.1088/0022-3727/46/23/235102

Flexible low-voltage pentacene memory thin-film transistors with combustion-processable Al_2O_3 gate dielectric and Au nanoparticles

Hyeon Jun Ha, Shin Woo Jeong, Tae-Yeon Oh, Minseok Kim, Kookhyun Choi, Jung Ho Park and Byeong-Kwon Ju

Display and Nanosystem Laboratory, College of Engineering, Korea University, Anam-dong, Seongbuk-Gu, Seoul, 136-713, Republic of Korea

E-mail: bkju@Korea.ac.kr (B-K Ju)

Received 21 January 2013, in final form 2 April 2013
Published 17 May 2013
Online at stacks.iop.org/JPhysD/46/235102

Abstract

A Au nanoparticles (NPs) embedded pentacene thin-film transistor (TFT) with solution-based Al_2O_3 was fabricated on a polyethersulfone substrate. The TFT for low-voltage operation within −3 V was realized with the Al_2O_3 dielectric film. By a combustion process for Al_2O_3, efficient driving of conversion reaction at low annealing temperature of 200 °C can be achieved and the device can be made on a plastic substrate. And, the Au NPs were deposited by the contact printing method using the polydimethylsiloxane stamp. From the electrical characteristics of the devices, a saturation mobility value of 4.25 $cm^2 V^{-1} s^{-1}$, threshold voltage (V_{th}) of ∼0.5 V, subthreshold swing of 70 mV dec^{-1} and memory window of 0.21 V at −3 V programming gate bias voltage were obtained.

(Some figures may appear in colour only in the online journal)

1. Introduction

Among the various organic semiconductor materials, pentacene is a promising material because of its higher saturation mobility than other materials [1–3]. Thus, pentacene is commonly used as a channel layer for organic nano-floating gate memory (NFGM) devices [4–6]. However, most pentacene-based NFGM devices have a large operating voltage because they use relatively thick organic gate-dielectric layers of low dielectric constant, which demand high power consumption [7, 8]. This large operating voltage is not suitable for practical NFGM devices that are applied in mobile electronics [7]. Moreover, these organic dielectric layers have an electrical weakness due to structural imperfections, including pinholes that are created during the deposition process [9, 10]. In recent years, alternative approaches to obtain low operating voltages for thin-film transistor (TFTs) have been reported using metal oxides such as Al_2O_3, CeO_2, TiO_2 and Y_2O_3 [9–12]. With the use of Al_2O_3 as dielectric films grown by physical vapour deposition (PVD) or atomic layer deposition (ALD), leakage current has also been sufficiently low [12, 13]. The problems of low dielectric-constant and thick gate-dielectric layer are solved with Al_2O_3 dielectric films, but most Al_2O_3 dielectric films fabricated by the PVD and ALD methods are limited to vacuum conditions, which are incompatible with solution processes. A solution process is necessary for large area coating and high throughput because it is simple and low cost and also the process temperature should be as low as possible to be used for bendable and durable plastic substrates [14–17].

In this paper, we report on the low operating voltage and high performance of the pentacene-based TFT using an Al_2O_3 dielectric film grown via a solution-based combustion process on a plastic substrate for NFGM devices. Al_2O_3 dielectric films have high dielectric constants (between 7.5 and 9.5) and mechanical flexibility and can be easily processed on different types of substrates [17]. To efficiently drive the conversion reaction at low annealing temperatures of Al_2O_3, we use a solution-based combustion process. The combustion process using urea or acetylacetone as fuel is widely used for energy-efficient synthesis of bulk materials such as semiconductors, carbides and binary oxides [18]. We designate the Al_2O_3

 © 2013 IOP Publishing Ltd Printed in the UK & the USA

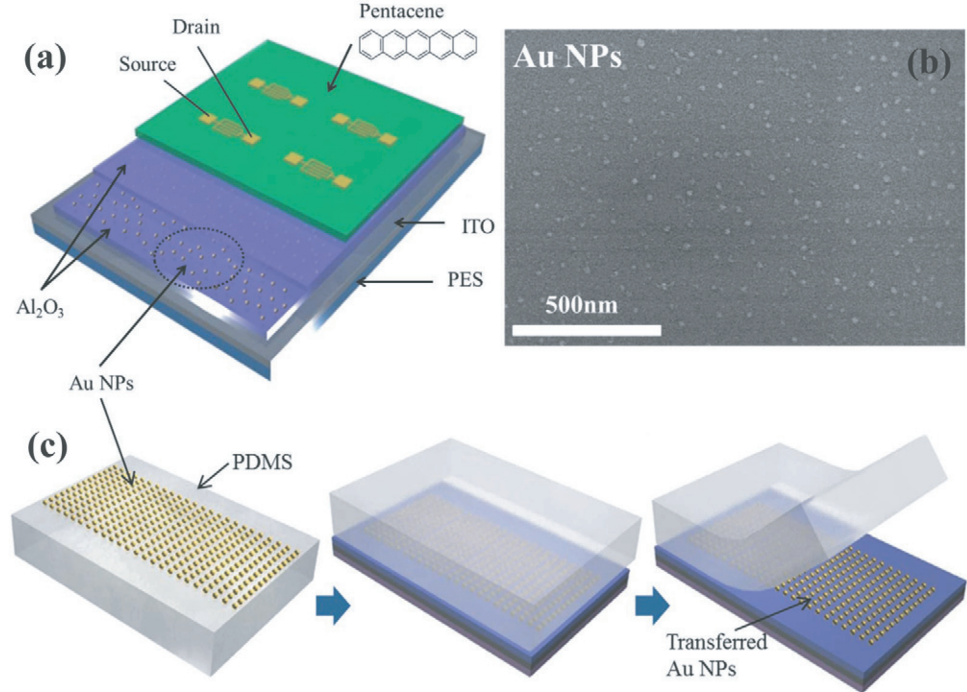

Figure 1. (*a*) Schematic diagram of the NFGM with pentacene, Al_2O_3 and Au NPs, (*b*) SEM image of Au NPs on Al_2O_3 surface, (*c*) process flow of Au NPs transfer by the contact printing method.

dielectric film using only Al precursor as Al_2O_3-α dielectric film and the Al_2O_3 dielectric film made by solution-based combustion process with urea as a combustion Al_2O_3 dielectric film. In addition, we explore memory properties through Au nanoparticle (NP) layer as charge-trapping elements in NFGM devices. Au NPs are most widely used for floating gate in NFGM devices because they are chemically stable, easily synthesized and have a high work function [4, 6]. To make Au NP layers, the contact printing process is used because it is a simpler and cheaper process than the other conventional techniques such as thermal deposition, photolithography and etching processes [19]. Thus, our devices can have low operating voltages and execute threshold voltage shifts for writing and erasing operations.

2. Experimental

The ITO-coated polyethersulfone (PES) substrate (i-Component Co., Ltd) is used as the functional plastic substrate, which has a glass temperature of above 230 °C. The ITO thickness is about 400 nm and the sheet resistance is around 20 Ω/square. And, the substrates were cleaned using isopropanol and deionized water in an ultrasonic bath. Then, the combustion Al_2O_3 solution was prepared by adding aluminum nitrate nonahydrate ($AlN_3O_9 \cdot 9H_2O$, aluminum precursor) and urea (CH_4N_2O) into 2-methoxy ethanol to a concentration of 0.1 M [16, 18]. The Al_2O_3-α solution was made by adding only aluminum precursor into 2-methoxy ethanol to a concentration of 0.1 M. By adding urea as a fuel into the combustion Al_2O_3 solution, the conversion process can efficiently drive the reaction to completion at a low annealing temperature because urea addition consumes the self-generated heat [18]. The solution of Al_2O_3 was filtered through a 0.45 μm membrane filter before spin coating. To disperse the Au NPs (purchased from British Bio Cell International) on the substrate, citrate coating and the Langmuir–Blodgett (LB) method are used [20, 21]. For citrate coating on Au NPs, aqueous 1 M citrate solution and gold colloid were mixed at a volume ratio of 1 : 1 in a 1.5 ml micro-centrifuge tube [6]. Then, this mixed solution was filtered using a centrifuge process. The filtered citrate-coated Au NPs were suspended in deionized water.

Before transferring the Au NPs on the substrate, first a blocking combustion Al_2O_3 dielectric film was deposited on the ITO/PES substrate. The ITO/PES substrate was treated in the oxygen plasma chamber (Cute plasma system; Femto Science, Korea) for 5 min. This treatment is important for improving the adhesion between the Al_2O_3 dielectric film and the ITO/PES substrate that leads to a uniform Al_2O_3 dielectric film [22]. The filtered Al_2O_3 solution was spin coated on the substrate as a blocking layer at 3000 rpm for 30 s. Then, the prepared samples were annealed at 200 °C for 10 min [18]. These spin coating and annealing processes were repeated twice for the blocking combustion Al_2O_3 dielectric film. On the blocking combustion Al_2O_3 dielectric film, the Au NPs were transferred by the contact printing method using the polydimethylsiloxane (PDMS) stamp. After that, the tunnelling combustion Al_2O_3 dielectric film was coated once. These combustion Al_2O_3 films were stabilized at 200 °C for 6 h. As a result, the blocking and tunnelling combustion Al_2O_3 dielectric films (have dielectric constant of 11.1) were spin-coated with thicknesses of 100 nm and 10 nm, respectively. Lastly, a 70 nm thick pentacene active layer and 80 nm gold source/drain electrodes were deposited by thermal evaporation. The comb-type source/drain electrodes had a channel width (W) and length (L) of 3000 μm and 120 μm, respectively. The transistor characteristics and

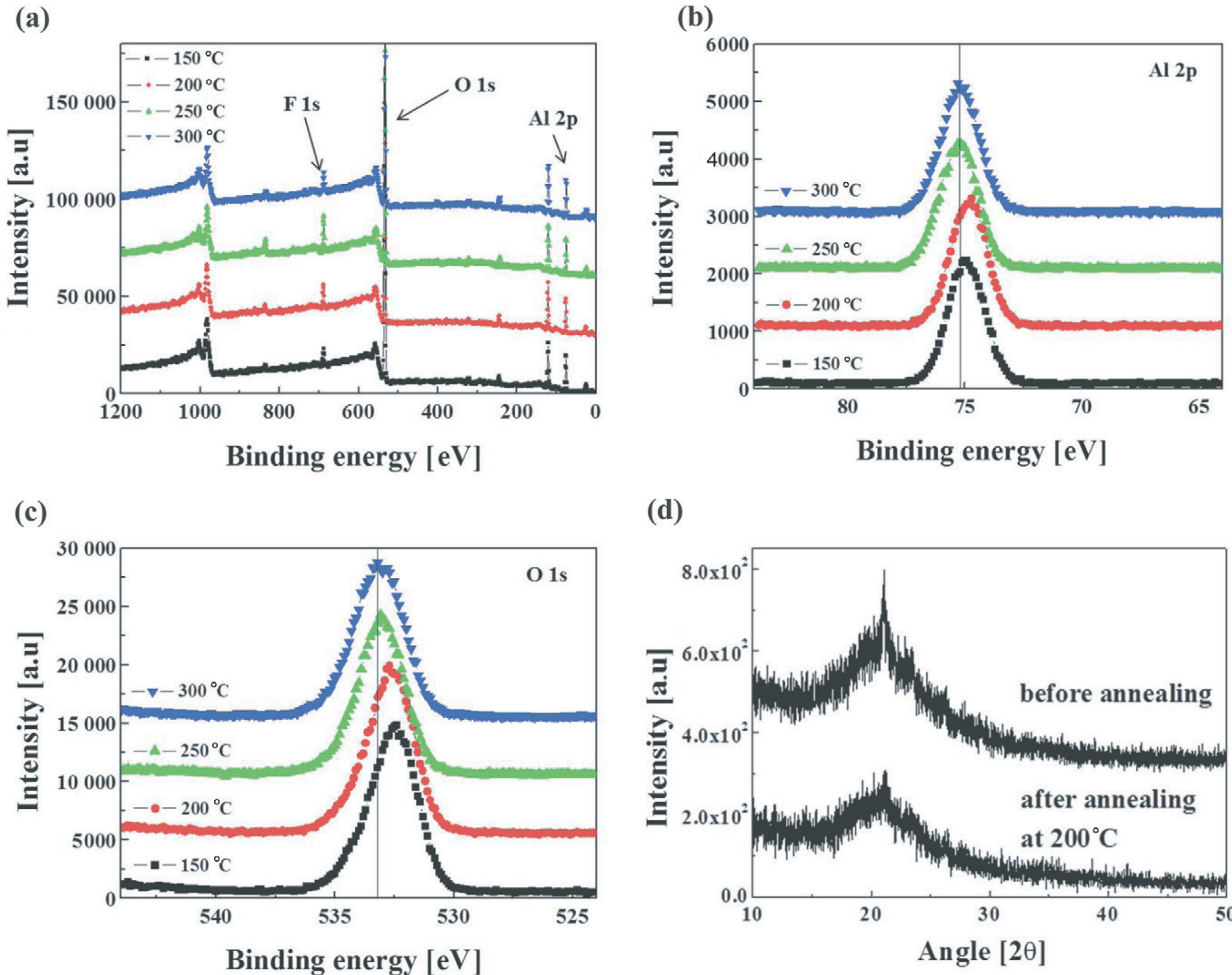

Figure 2. (*a*) XPS spectra of the combustion Al_2O_3 film for different temperatures, (*b*) XPS spectra of Al 2p peak and (*c*) O 1s peak. (*d*) XRD spectra of the combustion Al_2O_3 film before annealing (top), and after 200 °C annealing (bottom).

programmable memory properties were measured by the Keithley-4200 semiconductor parameter analyser at room temperature.

3. Results and discussion

Figure 1(*a*) shows a schematic illustration of the NFGM device structure for a staggered type TFT with the bottom gate on plastic substrates. The images of the Au NPs charge trapping layer were obtained by scanning electron microscopy (SEM). Figure 1(*b*) shows the SEM image of the Au NPs layer on the Al_2O_3 dielectric films surface. From the SEM image, we can estimate that the contact printing with citrate coating and LB technique process produced a nearly uniform monolayer. The average diameter and the density of the synthesized Au NP were 10 ± 2 nm and 2.03×10^{10} cm^{-2}, respectively. The Au NPs layer was made using the contact printing method. First, the Au NPs layer was made on a PDMS by the LB technique and this Au NPs layer on the PDMS was dried with N_2 gas. After the drying process, the Au NPs were transferred onto the Al_2O_3/ITO/PES substrate by controlling the detaching velocity as well as the surface energy of the stamp, as shown in figure 1(*c*).

Figures 2(*a*)–(*c*) of the x-ray photoelectron spectroscopy (XPS) analysis show the element components in the combustion Al_2O_3 films. The quantitative results according to the XPS relative at% show the ratio of Al/O as 2 : 3.34 (Al_2O_3 dielectric films are annealed at 200 °C), which is close to the composition ratio of Al_2O_3. The XPS Al 2p peak and XPS O 1s peak of alumina are detected at ~75 eV and ~533 eV, respectively, as shown in figures 2(*b*) and (*c*). These peak positions are consistent with previous reported values in the literature [24, 25]. As the annealing temperature is increased from 150 to 300 °C, the Al 2p and O 1s peak positions are shifted towards the high binding energy. These results indicate that the –Al–O–Al– matrix has a higher covalent character at higher temperatures [18]. Our devices used the 200 °C annealing temperature process because temperatures over 200 °C are not proper for application to the PES substrate. And figure 2(*d*) shows the x-ray diffraction (XRD) spectra of the combustion Al_2O_3 film before and after annealing. After the 200 °C annealing process, the narrowing peak was disappeared and this means that the Al_2O_3 film was transformed to an amorphous phase. This amorphous phase of Al_2O_3 film was correspond with other Al_2O_3 films that made at low temperature by ALD process (33–177° C) or sol-gel

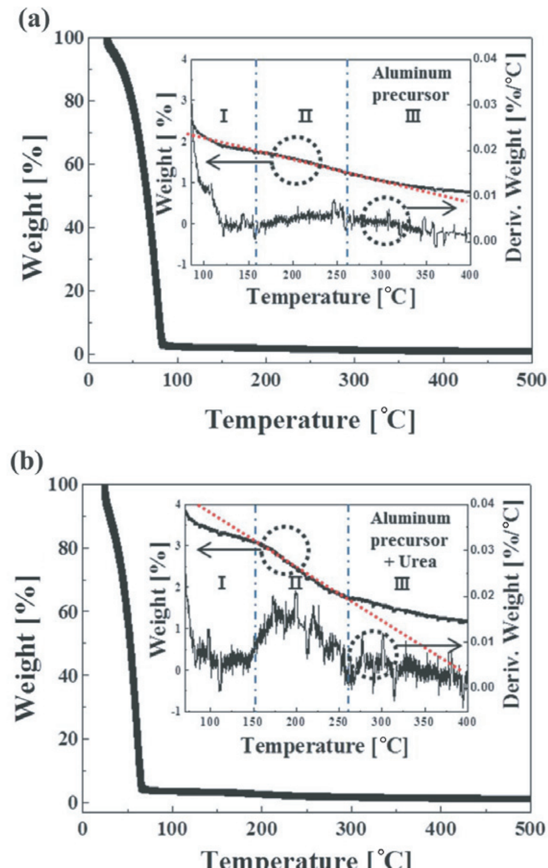

Figure 3. TGA diagrams of (*a*) 1.0M aluminum precursor without urea in 2-methoxy ethanol and (*b*) 1.0M aluminum precursor with urea in 2-methoxy ethanol and the insets show an enlarged view of each diagram.

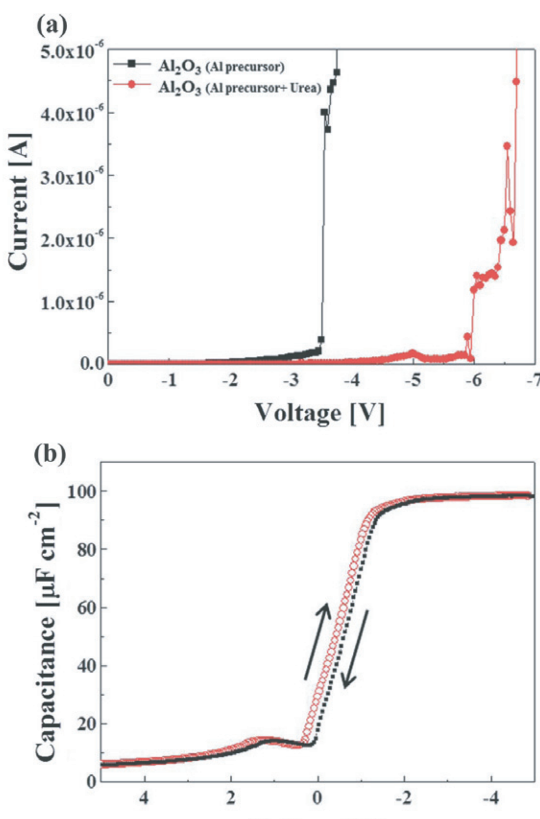

Figure 4. (*a*) Voltage-dependent current and of the 100 nm Al_2O_3-α and combustion Al_2O_3 dielectric film in metal–insulator–metal structure. (*b*) Voltage-dependent capacitance of the 100 nm combustion Al_2O_3 dielectric film in metal–insulator–semiconductor structure.

method (300 °C) [14, 23]. These XRD spectra transition in the annealing process certified that the aluminum precursor sufficiently formed the Al_2O_3 films by combustion process at a low annealing temperature of 200 °C.

Figures 3(*a*) and (*b*) show the thermogravimetric analysis (TGA) graphs for 1.0 M aluminum precursor without urea in 2-methoxy ethanol and (*a*) and 1.0 M aluminum precursor with urea in 2-methoxy ethanol (*b*). These graphs demonstrate the weight (in percent) dependence on the temperature measured from TGA performed under a N_2 ambient atmosphere as the samples were heated form about 21 to 500 °C at a heating rate of 10 °C min^{-1}. And the enlarged views of the temperature range 100–400 °C are presented in the inset of figures 3(*a*) and (*b*) [26, 27]. Figures 3(*a*) and (*b*) consist of three weight reduction sections. The first mass weight reduction in the range from 21 °C to part I region is most likely due to evaporation of 2-methoxy ethanol solvent (boiling point is 124–125 °C). And there is weight reduction rate change in part II due to the aluminum precursor chemical change, which is decomposed to oxide at a temperature around 150 °C, as presented in the inset of figures 3(*a*) and (*b*) [16]. This weight reduction rate of aluminum precursor with urea solution is faster than just an aluminum precursor solution because urea as a fuel accelerates this thermal reaction [18]. After reaction of part II the weight reduction process is continued at a slow rate in part III. The TGA analysis confirmed that the combustion process with urea for the Al_2O_3 dielectric film at 200 °C annealing temperature drives the conversion reaction more efficiently than the Al_2O_3-α dielectric process.

Current–voltage (I–V) characteristics of the Al_2O_3-α dielectric film and the combustion Al_2O_3 dielectric film were shown in figure 4(*a*). The top electrode area is 2.8×10^{-7} m^2. The Al_2O_3-α dielectric film was fabricated in the same way as the combustion Al_2O_3 dielectric film. The I–V characteristic of the combustion Al_2O_3 dielectric film showed better performance as a gate insulator than the Al_2O_3-α dielectric film in leakage current and breakdown voltage. The leakage currents of the Al_2O_3-α dielectric film and the combustion Al_2O_3 dielectric film were 1.29×10^{-7} A and 3.46×10^{-9} A, respectively, at −3 V. The break voltage of the combustion Al_2O_3 dielectric film was −6 V which is about twice larger than that of Al_2O_3-α dielectric film. Figure 4(*b*) shows the capacitance–voltage (C–V) characteristics of the combustion Al_2O_3 dielectric film. The C–V measurements were carried out on metal–insulator–semiconductor structures for the combustion Al_2O_3 dielectric film at 100 kHz and capacitance was about 98.2 μF cm^{-2}. The dielectric constant is 11.1 and this value is calculated by the equation $C = \varepsilon_r \varepsilon_0 A/d$, where C is the capacitance; ε_r is the dielectric constant; $\varepsilon_0 = 8.854 \times 10^{-12}$ F m^{-1} is the permittivity of free space; $A = 2.8 \times 10^{-7}$ m^2 is capacitor area; and $d = 100$ nm

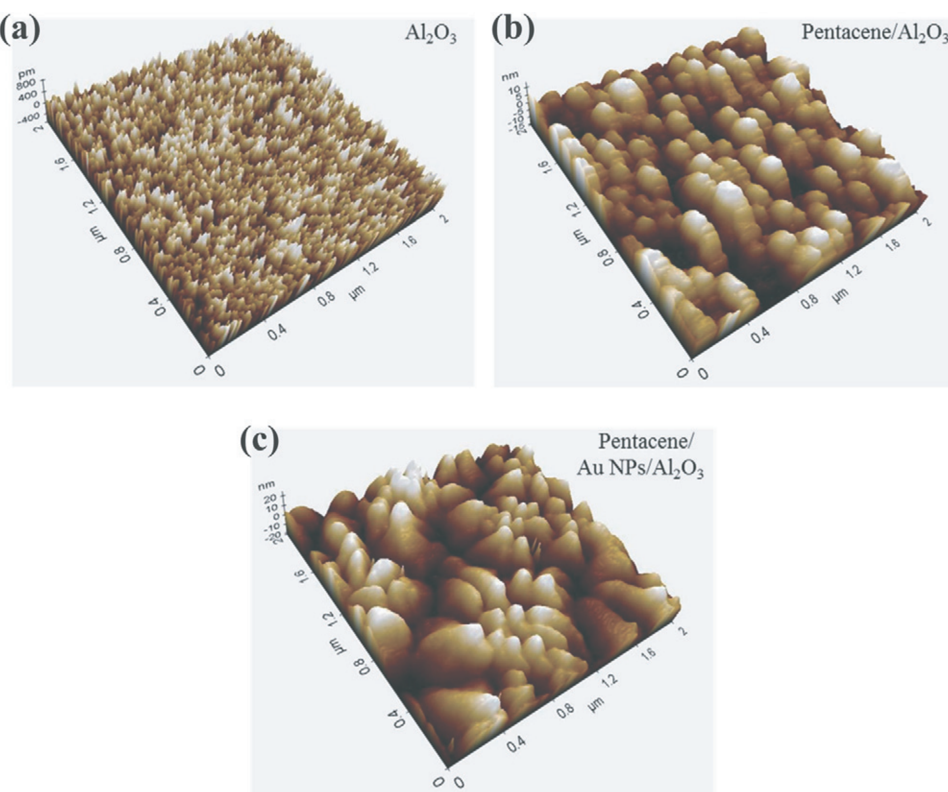

Figure 5. AFM images of (*a*) the combustion Al_2O_3 film, (*b*) the pentacene film deposited on combustion Al_2O_3 and (*c*) the pentacene film deposited on Au NPs/Al_2O_3.

is the dielectric film thickness. We found similar behaviour for Al_2O_3-α dielectric film.

Figure 5(*a*) shows the atomic force microscope (AFM) image of the combustion Al_2O_3 surface. The peak-to-valley value and the root mean square (rms) roughness were 0.95 and 0.11 nm, respectively. Therefore, the combustion Al_2O_3 dielectric films have very smooth surfaces [14]. The AFM images of the pentacene film deposited on Al_2O_3 and Au NPs/Al_2O_3 were shown in figures 5(*b*) and (*c*). The rms roughnesses of those pentacene films were 4.73 nm and 7.79 nm, respectively. The pentacene film deposited on Au NPs/Al_2O_3 had bigger grain size than Al_2O_3 because the pentacene grains were grown easily around a core of Au NPs [28].

In many studies of NFGM devices, Au NPs as the floating gate exhibited good memory effects by trapping/detrapping charge carriers (holes and electrons) [6]. According to figures 6(*a*)–(*c*), the charging/discharging states of the Au NPs change the memory window (threshold voltage (V_{th}) shift) [29]. With a negative gate bias pulse, hole charge carriers tunnel through the tunnelling Al_2O_3 dielectric film from pentacene to the Au NPs. And these hole charge carriers become trapped in the Au NPs; this is called the 'programming' process, as shown in figure 6(*a*). In the 'storage' state, as shown in figure 6(*b*), the charging Au NP layer makes the V_{th} shift. On the other hand, when a positive gate bias pulse is applied in the 'erasing' process, the hole charge carriers are de-trapped from the Au NPs to the pentacene layer, as shown in figure 6(*c*). And this discharging of Au NP layer makes V_{th} shift to the initial state. The injection of the hole charge carriers through the tunnelling dielectric layer in the programming/erasing process can be attributed to the Fowler–Nodheim tunnelling.

$$\mathrm{EOT} = t_{\text{high-}k}\left(\frac{k_{\mathrm{SiO_2}}}{k_{\text{high-}k}}\right), \quad (1)$$

where EOT is the equivalent oxide thickness; $t_{\text{high-}k}$ is the thickness of the Al_2O_3 dielectric film; $k_{\mathrm{SiO_2}}$ is the dielectric constant of the SiO_2 dielectric film; and $k_{\text{high-}k}$ is the dielectric constant of the Al_2O_3 dielectric film. By equation (1), the 10 nm tunnelling Al_2O_3 dielectric film has an EOT of 3.91 nm. A dielectric layer which has a sub-4.5 nm EOT [30] and a gate bias voltage of above 1 V for 1 s can lead to Fowler–Nodheim tunnelling [30].

Figures 7(*a*) and (*b*) show the output and transfer characteristics of Au/pentacene/Al_2O_3/ITO/PES. Pentacene-based TFTs were fabricated without Au NPs to clarify the low voltage operation of the combustion Al_2O_3 gate dielectric film at the annealing temperature of 200 °C. The saturation mobility was calculated by the following equation (2). V_{th} was determined from the intercept of the plot of $(I_D)^{1/2}$ versus V_G [7, 16].

$$I_D = \left(\frac{C_i \mu_{sat} W}{2L}\right)(V_G - V_{th})^2 \qquad \text{for } V_D > V_G - V_{th}, \quad (2)$$

where I_D is the source-to-drain current; C_i is the capacitance per unit area of the gate-insulator; μ_{sat} is the saturation mobility; W and L are the channel width and length, respectively; V_G is the gate voltage; and V_D is the source-to-drain voltage. The pentacene-based TFTs showed a μ_{sat} of

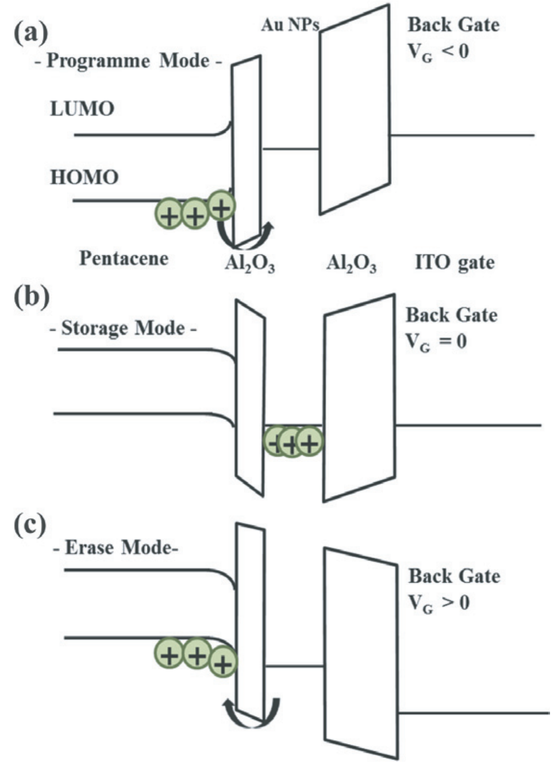

Figure 6. Schematic energy-band diagrams of pentacene/Al_2O_3/Au NPs/Al_2O_3/Au gate (*a*) program mode, (*b*) storage mode and (*c*) erase mode.

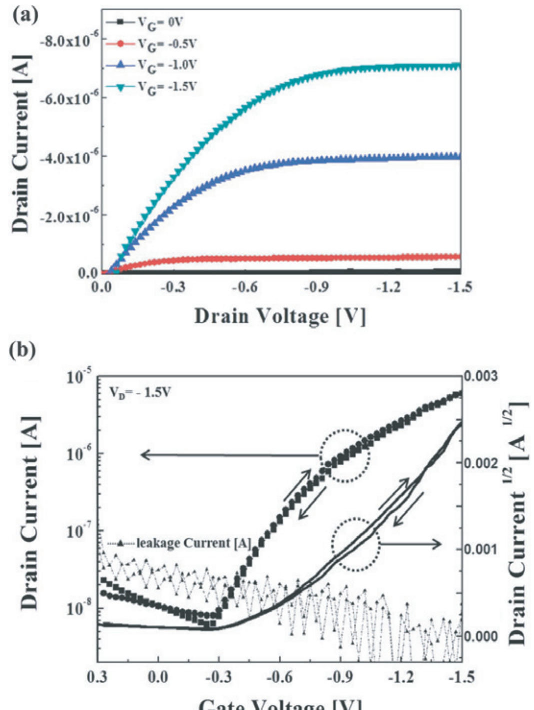

Figure 7. (*a*) Output characteristics and (*b*) transfer characteristics of the Au/pentacene/ Al_2O_3/ITO/PES TFT without Au NPs.

$4.25\,cm^2\,V^{-1}\,s^{-1}$, sub-threshold swing of $70\,mV\,dec^{-1}$, V_{th} of ~ 0.5 V and on–off drain current ratio of $\sim 10^3$. The variation of the transfer characteristics upon a gate voltage sweep was negligible because of the fine combustion Al_2O_3 dielectric film deposition, which implies a low interface trap charge between the pentacene and the combustion Al_2O_3. But the off-current was higher than those of the other TFTs with Al_2O_3 dielectric films [12, 13]. This high off-current phenomenon is often seen in TFTs fabricated with solution Al_2O_3 dielectric films on ITO [14, 16]. The off current can be improved by self-assembled monolayer (SAM) treatment and gate patterning, which can reduce the overlap of the source–drain and gate area [9, 13].

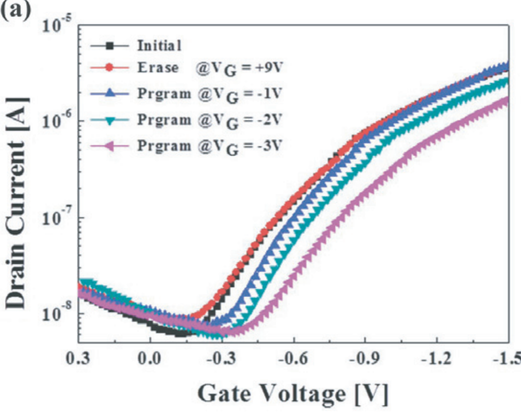

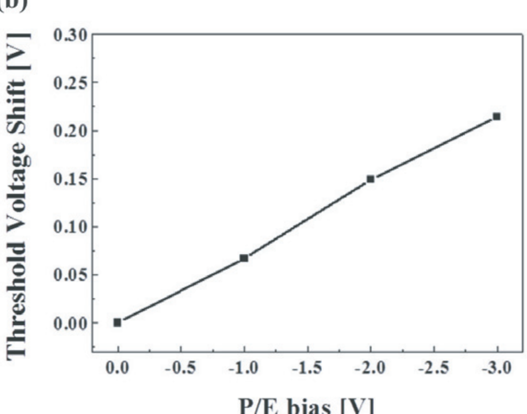

Figure 8. (*a*) Transfer characteristics of the transistor at different programming voltages, (*b*) V_{th} shift measured at different V_G bias pulse ranges from programming voltage of −1, −2, −3 V to erasing voltage of 9 V for 1 s.

The NFGM devices with Au NPs showed memory effects, as shown in figures 8(*a*) and (*b*). These NFGM devices had a structure of Au/pentacene/Al_2O_3/Au NPs/Al_2O_3/ITO/PES. The grain boundary density of pentacene was decreased by Au NPs but the I_D values at NFGM were a little lower than the I_D values of the pentacene-based TFTs. Au NPs which act as impurities in the pentacene film decreased the charge transport in the channel for pentacene TFTs [31]. When different negative gate voltage biases were applied to programming, the transfer curve shifted towards the negative direction. After the erasing operation with more than +9 V gate voltage bias for 1s, the transfer curve was located in almost the same position as the initial transfer curve, as shown in figure 8(*a*). The V_{th} shift increased from 0.06 to 0.21 V depending on the range of programming voltage bias from −1 to −3 V for 1 s, as shown in figure 8(*b*). The maximum V_{th} shift value of 0.21 V was achieved at −3 V gate bias voltage. This value of V_{th} shift was

reasonable when compared with those in other reports in terms of the operation voltage [32, 33].

4. Conclusions

In conclusion, flexible and low operating voltage NFGM devices were fabricated with Au NPs and combustion Al_2O_3 dielectric films. These NFGM devices exhibited large memory windows and high saturation mobility at low operating voltages. Additionally, the Al_2O_3 dielectric films were efficiently fabricated by the solution-based combustion process at a low temperature. And the Au NPs layer was deposited by the contact printing method without damaging the Al_2O_3 dielectric film. Therefore, the NFGM devices fabricated by these techniques have great potential for low-power consumption memory devices on plastic substrates.

Acknowledgments

This work was partly supported by the IT R&D Programme of MOTIE/KEIT (KI002104, Development of Fundamental Technologies for Flexible Combined-Function Organic Electronic Device), the Industrial-Educational Cooperation Programme between Korea University and Samsung Electronics and the Basic Science Research Programme through the National Research Foundation of Korea (NRF) funded by the Ministry of Education, Science and Technology (MEST) (CAFDC-20120000816).

References

[1] Puigdollers C V J, Martin I, Orpella A, Vetter M and Alcubilla R 2004 *J. Non-Cryst. Solids* **338** 617
[2] Kitamura M and Arakawa Y 2008 *J. Phys.: Condens. Matter* **20** 184011
[3] Simeone D, Cipolloni S, Mariucci L, Rapisarda M, Minotti A, Pecora A, Cuscuna M, Maiolo L and Fortunato G 2009 *Thin Solid Films* **517** 6283
[4] Kim S J, Song J M and Lee J S 2011 *J. Mater. Chem.* **21** 14516
[5] Scott J C and Bozano L D 2007 *Adv. Mater.* **19** 1452
[6] Kim H J, Jung S M, Kim Y H, Kim B J, Ha S, Kim Y S, Yoon T S and Lee H H 2011 *Thin Solid Films* **519** 6140
[7] Facchetti A, Yoon M H and Marks T J 2005 *Adv. Mater.* **17** 1705
[8] Shin W C, Moon H, Yoo S, Li Y X and Cho B J 2010 *IEEE Electron. Device Lett.* **31** 1308
[9] Halik M, Klauk H, Zschieschang U, Schmid G, Dehm C, Schutz M, Maisch S, Effenberger F, Brunnbauer M and Stellacci F 2004 *Nature* **431** 963
[10] Hwang D K, Kim C S, Choi J M, Lee K, Park J H, Kim E, Baik H K, Kim J H and Im S 2006 *Adv. Mater.* **18** 2299
[11] Klauk H, Zschieschang U, Pflaum J and Halik M 2007 *Nature* **445** 745
[12] Majewski L A, Schroeder R and Grell M 2005 *Adv. Mater.* **17** 192
[13] Zhang X H, Domercq B, Wang X D, Yoo S, Kondo T, Wang Z L and Kippelen B 2007 *Org. Electron.* **8** 718
[14] Avis C and Jang J 2011 *J. Mater. Chem.* **21** 10649
[15] Jeong S and Moon J 2012 *J. Mater. Chem.* **22** 1243
[16] Pal B N, Dhar B M, See K C and Katz H E 2009 *Nature Mater.* **8** 898
[17] Rahman M A *et al* 2012 *J. Nanosci. Nanotechnol.* **12** 1348
[18] Kim M G, Kanatzidis M G, Facchetti A and Marks T J 2011 *Nature Mater.* **10** 382
[19] Kim J W, Yang K Y, Hong S H and Lee H 2008 *Appl. Surf. Sci.* **254** 5607
[20] Li Y J, Huang W I J and Sun S G 2006 *Angew. Chem. Int. Edn Engl.* **45** 2537
[21] Wang Y L, Chen H J and Wang E K 2008 *Nanotechnology* **19** 105604
[22] Sunkara V, Park D K, Hwang H, Chantiwas R, Soper S A and Cho Y K 2011 *Lab Chip* **11** 962
[23] Groner M D, Fabreguette F H, Elam J W and George S M 2004 *Chem. Mater.* **16** 639
[24] Sohal R, Lupina G, Seifarth O, Zaumseil P, Walczyk C and Schroeder T 2010 *Surf. Sci.* **604** 276
[25] Zhang Q Y, Wang P S, Zhao W J and Wang L 2000 *Surf. Coat. Techol.* **128** 121
[26] Mathieu Y, Vidal L, Valtchev V and Lebeau B 2009 *New J. Chem.* **33** 2255
[27] Shih T S and Liu Z B 2006 *Mater. Trans.* **47** 1347
[28] Shtein M, Mapel J, Benziger J B and Forrest S R 2002 *Appl. Phys. Lett.* **81** 268
[29] Tseng C W, Chen Y L and Tao Y T 2012 *Org. Electron.* **13** 1436
[30] Govoreanu B, Brunco D P and Van Houdt J 2005 *Solid State Electron.* **49** 1841
[31] Jurchescu O D, Baas J and Palstra T T M 2004 *Appl. Phys. Lett.* **84** 3061
[32] Cheng C H, Yeh F S and Chin A 2011 *Adv. Mater.* **23** 902
[33] Kaltenbrunner M, Stadler P, Schwodiauer R, Hassel A W, Sariciftci N S and Bauer S 2011 *Adv. Mater.* **23** 4892